

Fabrication of fluorescent cellulose nanocrystal via controllable chemical modification towards selective and quantitative detection of Cu(II) ion

Yan-Jie Zhang · Xiao-Zhou Ma · Lin Gan · Tao Xia · Jun Shen · Jin Huang

Received: 21 June 2018 / Accepted: 13 August 2018 / Published online: 23 August 2018
© Springer Nature B.V. 2018

Abstract Fluorescent cellulose nanocrystals (fCNCs) have shown a great potential as optical probe for the applications of bioimaging or metal ion detection. In this work, by a controllable esterification strategy, the cellulose nanocrystal (CNC) surface was modified with ethylenediaminetetraacetic dianhydride (EDTAD) to achieve highly carboxylation degree, and, meanwhile, keep surface integration and crystalline structure in comparison with the TEMPO oxidation method. Then, the controllability of carboxylation degree was applied to produce a series of fCNCs with various conjugating

densities of fluorescent 7-amino-4-methylcoumarin (AMC). The steric effect of AMCs on the fCNC surface could inhibit self-quenching, resulting in a more stable fluorescence intensity independent upon the change of fCNC concentration and a relatively high quantum efficiency in the solid state. Moreover, the fluorescence signals of fCNC can be selectively affected by Cu^{2+} , and even high Cu^{2+} concentration resulted in the visualized color change from blue to purple under ultraviolet radiation. Hence, two linear correlations with the Cu^{2+} concentration, i.e. the fluorescence attenuation ratio at 390 nm in 0.5–16 ppm of Cu^{2+} concentration and the fluorescence intensity ratio of 440 nm versus 390 nm in 16–160 ppm of Cu^{2+} concentration, contributed to a potential of quantitative Cu^{2+} detection. Especially, the on–off behavior of the fCNC fluorescence at the critical Cu^{2+} concentration of 0.5 ppm was well consistent with the requirement of the Guideline of Drinking-Water Quality (GDWQ) administrated by World Health Organization (WHO), and hence might be used to rapid and visualized evaluation of drinking water quality. This work provides a new fluorescent nanomaterial that can be used in metal ion detection. Furthermore, the nontoxicity, biodegradability and environment-friendliness of cellulose nanocrystals might also contribute to the additional advantages for the application of environmental surveillance.

Yan-Jie Zhang and Xiao-Zhou Ma have contribute equally to this work.

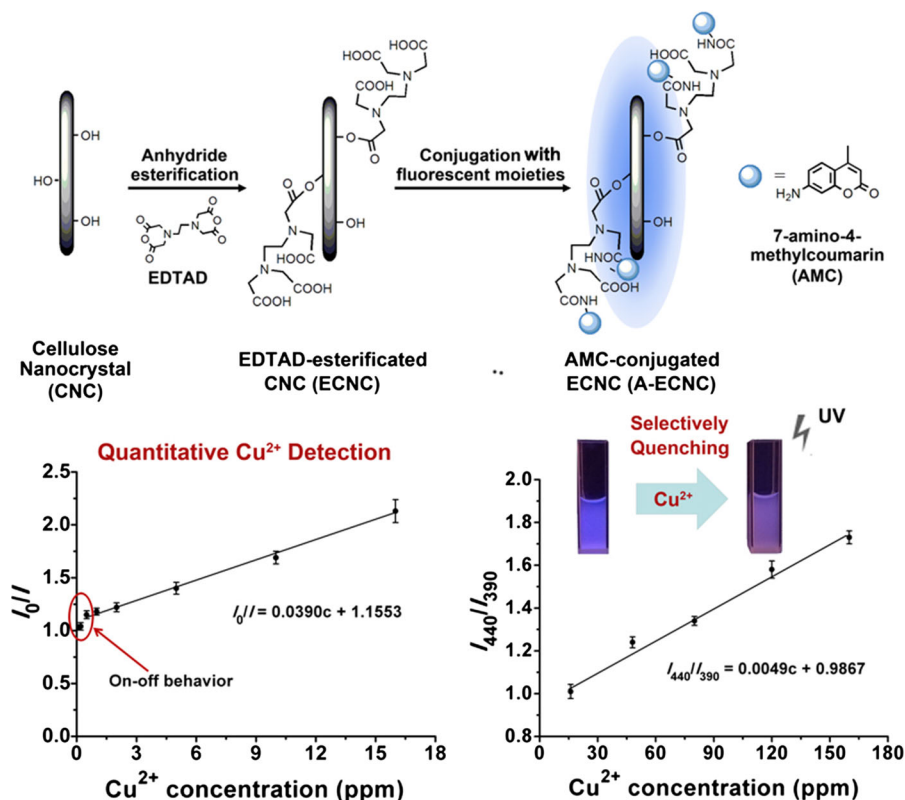
Electronic supplementary material The online version of this article (<https://doi.org/10.1007/s10570-018-1995-9>) contains supplementary material, which is available to authorized users.

X.-Z. Ma · L. Gan · J. Huang (✉)
School of Chemistry and Chemical Engineering,
Southwest University, Chongqing 400715, China
e-mail: huangjin@iccas.ac.cn;
huangjin2015@swu.edu.cn

Y.-J. Zhang · T. Xia · J. Huang
School of Chemistry, Chemical Engineering and Life
Sciences, Wuhan University of Technology,
Wuhan 430070, China

J. Shen
Chongqing Institute of Green and Intelligent Technology,
Chinese Academy of Science, Chongqing 400715, China

Graphical abstract



Keywords Cellulose nanocrystal · Chemical modification · Fluorescent detection · Quantitative detection of metal ion

Introduction

Cellulose nanocrystal (CNC) has been widely emerging as environment-friendly material enhancer, drug excipient and other applications for its biodegradability, high biocompatibility and nontoxicity (Xue et al. 2017). The hydroxyl groups on CNC surface contribute a good flexibility to facile modification (Ma et al. 2017; Sunasee et al. 2016). Hence, the CNCs could conjugate with fluorescent molecules, and be applied as the optical probe for bioimaging or ion detection. The pioneering preparation of such fluorescent cellulose nanocrystal (fCNC) was carried out by a strategy of three-step reaction. So the CNC firstly reacted with epichlorohydrin to decorate epoxy ring on the CNC surface followed by opening epoxy ring

with ammonium hydroxide to introduce amine group, and finally, the isothiocyanate groups of fluorescein-5-isothiocyanate (FITC) were covalently conjugated with the as-prepared aminated CNC surface (Dong and Roman 2007). Moreover, a “green” fCNC showed low cytotoxicity, and could be easily applied in cell labeling (Mahmoud et al. 2010). At the same time, more strategies were attempted to conjugate fluorescent molecules on the CNC surface (Grate et al. 2015; Sirbu et al. 2016; Xue et al. 2017). For example, the aminoethyl rhodamine (RhB) could be easily amidated onto the carboxylic surface of TEMPO-oxidized CNC via amidation reaction (Zhao et al. 2014) while the Alexa Fluor 633 and coumarin could be conjugated to the terminal aldehyde group of CNC via Schiff base reaction (Colombo et al. 2015; Huang et al. 2013). Recently, it was reported that the conjugation of Rhodamine B isothiocyanate (RBITC) onto the surface amine of CNC via carbamation affected quantum efficiency and emission wavelength (Ding et al. 2017).

Depending upon the advantages in the biocompatibility and nontoxicity of cellulose nanocrystals, the

fCNC has been applied in biomedical field, such as cell labelling mentioned above and even fluorescent *in vivo* imaging for the disease diagnosis (Seabra et al. 2018). In this case, the Alexa Fluor 633-modified fCNC was observed to enrich in the bone tissue *in vivo* without any effect on animal health after injection for 7 days, showing a great potential of bone disease diagnosis (Colombo et al. 2015). As regards to the cytotoxicity of fCNC containing the additional fluorescent moieties, the cell viability was verified to keep a higher level after being treated with the fCNC dose up to 140 $\mu\text{g}/\text{mL}$ for 48 h (Colombo et al. 2015; Seabra et al. 2018). The facile surface modification make rigid CNC plays a role of designable nanotemplate to introduce the specific fluorescent moieties and construct the matched spatial structure for target-detection molecules (Edwards et al. 2016; Fontenot et al. 2016). For example, the CNCs were modified by pyrene molecules for the attempt of quantitative Fe^{3+} detection. Although the pyrene-conjugated CNCs in aqueous media could not formed the excimers like those in organic solvents and only gave a relatively weak fluorescence intensity, those still showed a potential as the probe of Fe^{3+} detection depending upon a good linear correlation between fluorescent signal and Fe^{3+} concentration (Zhang et al. 2012).

Although the Cu^{2+} is essential for the metabolism of human body, excessive uptake of Cu^{2+} might cause several chronic diseases including Alzheimer's

disease, mucosal necrosis or liver damage (Awual 2017; Drew 2017; Kanumakala et al. 2002; Saleem et al. 2017; Uriu-Adams and Keen 2005). So the concentration of Cu^{2+} in drinking water should be strictly monitored while the rapid and facile method of Cu^{2+} detection is required. In this work, a new kind of coumarin-modified fCNC probe for selective and quantitative detection of Cu^{2+} in aqueous media was developed via a strategy of two-step reaction (Fig. 1), i.e. an esterification of ethylenediaminetetraacetic dianhydride (EDTAD) to produce the CNC with a highly carboxylated surface (ECNC) and a subsequent amidation with 7-amino-4-methylcoumarin (AMC) to give fluorescent AMC-amidated ECNC (A-ECNC). In this case, a mild condition and controllability of anhydride esterification are expected to maintain the integration of CNC surface in comparison with the TEMPO oxidation, and hence to regulate the grafting densities of AMC and optimize the fluorescence intensity of fCNC (Chen et al. 2009; Gan et al. 2017; Lin et al. 2009, 2012b). At the same time, the steric effect and colloid stability of rigid fCNC might contribute to prevent surface AMC from self-quenching, resulting in a stable fluorescence intensity independent upon the fCNC concentration. Furthermore, the fluorescence behaviors between A-ECNC and Cu^{2+} were investigated to explore the selectivity and quantitative detection potential of A-ECNC towards Cu^{2+} .

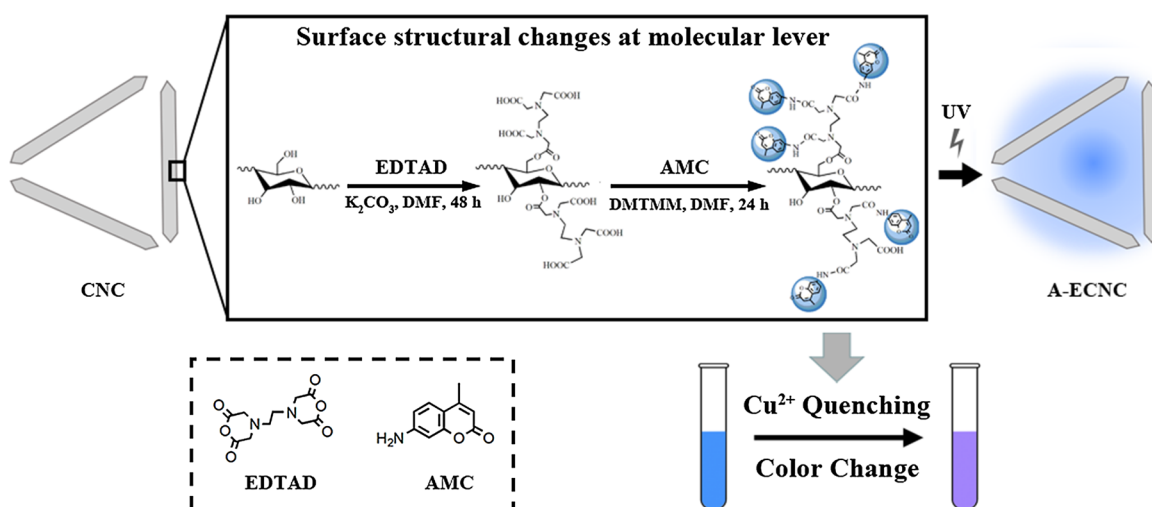


Fig. 1 Schematic illustration of molecular-level structural changes on the CNC surface in the synthesis process of fCNC, i.e. A-ECNC, with a potential of Cu^{2+} detection, and the visualized fluorescence and color changes induced by Cu^{2+} under UV radiation

Experimental section

Materials

Cotton linter was purchased from Weifang Yingfeng Cotton Co., Ltd. (China). Ethylenediaminetetraacetic dianhydride (EDTAD), 7-amino-4-methylcoumarin (AMC) and 4-(4,6-dimethoxy-1,3,5-triazin-2-yl)-4-methylmorpholinium chloride (DMTMM) were purchased from Aladdin (Shanghai, China). Potassium carbonate anhydrous (K_2CO_3), sodium hydroxide (NaOH, 96.0%), sodium carbonate anhydrous (Na_2CO_3 , 99.8%), sulfuric acid (H_2SO_4 , AR), hydrochloric acid (HCl, AR), ethanol (95%), methanol (99.5%), acetone (99.5%) and molecular sieves type 4 Å (Φ 3–5 mm) as well as $CuSO_4 \cdot 5H_2O$, $BaCl_2 \cdot 2H_2O$, $MgCl_2 \cdot 6H_2O$, $CaCl_2$, $CoCl_2 \cdot 6H_2O$, $ZnCl_2$, $MnSO_4$, $Pb(NO_3)_2$, $HgCl_2$, $NiCl_2 \cdot 6H_2O$, $FeCl_3 \cdot 6H_2O$, KCl and NaCl were obtained from Sinopharm Chemical Reagent Co., Ltd. (China). *N,N'*-Dimethylformamide (DMF, 99.8%) was purchased from Kemi Ou Chemical Reagent Co., Ltd. (Tianjin, China), and was dried over molecular sieves type 4 Å before used.

Preparation of cellulose nanocrystal

The cellulose nanocrystal (CNC) was extracted by acid hydrolysis according to the previous report (Lin and Dufresne 2014; Lin et al. 2012a). With an equivalent feeding ratio of 25 g fibers in 1000 mL solution, the cotton linter was firstly immersed in 2% w/v NaOH aqueous solution under a mechanical stirring for 12 h, and then filtered and rinsed with distilled water repeatedly until pH = 7. After drying in an oven, 12.5 g fibers were treated in 250 mL 64% v/v H_2SO_4 solution at 45 °C for 1 h under mechanical stirring. Subsequently, the suspension containing CNC was cooled in icy water bath, and washed with distilled water by successive centrifugations. After dialyzing for 5 days and freeze-drying, the CNC powder was obtained.

Synthesis of EDTAD-esterified CNC

The EDTAD-esterified CNC (ECNC) was prepared by a reaction between the anhydride group of EDTAD and the surface hydroxyl group of CNC. Firstly, 0.5 g CNC was added into 20 mL anhydrous DMF and treated by ultrasonic to give a homogeneous

suspension. Then, 20.7 mg K_2CO_3 was added into the CNC suspension, and conditioned at 75 °C under N_2 atmosphere for 30 min. Subsequently, the given amount of EDTAD was dispersed in 10 mL anhydrous DMF, and added into the above CNC suspension. The reaction carried out at 75 °C under N_2 atmosphere for 48 h. Thereafter, the resultant mixture was washed with DMF, Na_2CO_3 aqueous solution (10 wt %) and deionized water by centrifugation repeatedly. Finally, the precipitate was treated with a dilute hydrochloric acid solution (pH 4 ~ 6) for 45 min followed by the centrifugations in turn with distilled water, ethanol and acetone, and freeze-dried to produce ECNC. According to the feeding molar ratio of EDTAD versus hydroxyl groups on CNC surface, the as-prepared carboxylated CNC were respectively coded as ECNC/0.5, ECNC/2, ECNC/4, ECNC/10, ECNC/20 and ECNC/40, where the numbers represented the feeding molar ratio of EDTAD in contrast to the molar mass of hydroxyl groups on CNC surface.

Synthesis of fluorescent cellulose nanocrystals

Firstly, a mixture of ECNC (0.2 g) and 4-(4,6-Dimethoxy-1,3,5-triazin-2-yl)-4-methylmorpholinium chloride (DMTMM) was added into DMF and stirred at room temperature for 30 min. Subsequently, according to the carboxyl content of ECNC, the given amount of AMC with 5 times mole equivalent was added into the above mixture, and reacted for 24 h at 25 °C in darkness. Thereafter, the product was washed with DMF, acetone/distilled water mixture, methanol by successive centrifugations, and then dialyzed for 3 days to produce AMC-amidated ECNC (A-ECNC). Corresponding to the codes of initial EDTAD-esterified CNC, the resultant fluorescent CNCs were named as A-ECNC/0.5, A-ECNC/2, A-ECNC/4, A-ECNC/10, A-ECNC/20 and A-ECNC/40, respectively.

Characterization

Fourier transform infrared (FTIR) spectra were recorded on a Nicolet iS5 FTIR instrument (Nicolet, Madison, USA). Fluorescence spectra were recorded on an F-7000 fluorescence spectrometer (Hitachi, Japan) using excitation wavelength of 350 nm and 325 nm for the corresponding specimens while the quantum efficiency was measured on an FLS920P fluorescence spectrometer equipped with a 450 W

Xenon lamp (Edinburgh, England) using an excited wavelength of 325 nm. The UV spectra were measured by a UV-2600 spectrophotometer (Shimadzu, Japan). X-ray Diffraction (XRD) measurements were performed on a D/Max-III A X-ray diffractometer (Rigaku Denki, Tokyo, Japan) using Cu K α radiation ($\lambda = 0.02$ nm) at 40 kV and 60 mA. Transmission electron microscope (TEM) images were observed on a JEM 1200 EX microscope (JEOL, Japan) at an operating voltage of 120 kV. Elemental analysis was carried out on a Vario EL Cube Analyzer (Elementar, Germany). Conductivity titration were carried out using a STARTER 3100 C Conductimeter (OHAUS, USA). The ζ potential values of suspensions were determined by a Zetasizer Nano ZS90 (Malvern Instruments Ltd., Worcestershire, United Kingdom).

Fluorescence properties and ion quenching behaviors of fluorescent cellulose nanocrystals

The effects of AMC on fluorescence properties of A-ECNCs were investigated to select the optimal fCNC as ion detection probe while the dependence of fluorescence signals upon the fCNC concentration was also determined. Furthermore, the quenching possibility of metal ions towards fCNC was determined, and the used metal ions included Cu²⁺, Co²⁺, Ba²⁺, Mg²⁺, Ca²⁺, Zn²⁺, Mn²⁺, Pb²⁺, Hg²⁺, Fe³⁺, Na⁺ and K⁺. In the detection system, the concentrations of fCNC and metal ion were controlled as 0.1% w/v and 20 ppm, respectively. All the fluorescence measurement of fCNC were carried out using an excitation wavelength of 325 nm, and the fluorescence intensities at 390 nm were recorded.

Quantitative detection of Cu²⁺ using fluorescent cellulose nanocrystals

A series of aqueous solutions containing 0.1–3200 ppm Cu²⁺ were prepared, and the A-ECNC/2 was used as a fluorescence probe of detection. After adding the A-ECNC/2, the fluorescence spectra of every aqueous solutions with various Cu²⁺ concentrations were recorded using an excitation wavelength of 325 nm. Moreover, the changes of fluorescence intensities or intensity ratios at the predominant peaks were used to establish the linear correlation between the fluorescence signals and the Cu²⁺ concentrations.

Results and discussion

Fabrication of fluorescent cellulose nanocrystals

To achieve a high and controlled carboxyl degree without excess damage of crystalline structure and surface integration for cellulose nanocrystals (CNCs), the mild esterification was applied using the ethylenediaminetetraacetic dianhydride (EDTAD) as reactant. Then, a series of fluorescent cellulose nanocrystals (fCNCs) were prepared by amidation conjugating of 7-amino-4-methylcoumarin (AMC) onto the EDTAD-esterified CNC (ECNC) with various carboxyl degree. FTIR spectra in Fig. 2 were used to identify the structures of CNC, ECNC and their derivative fluorescent CNC, i.e. AMC-amidated ECNC (A-ECNC), with a comparison of CNC and AMC. In the spectrum of ECNC, the EDTAD esterification was proved by the emerging predominant peak located at 1743 cm⁻¹, which was assigned to the stretching vibration of C=O bond in the conjugated moiety of ethylenediaminetetraacetic acid. After conjugating AMC onto ECNC, the spectrum of A-ECNC showed two peaks located at 1530 cm⁻¹ and 1615 cm⁻¹, which corresponded to the N–H vibration and C–N stretching of newly formed amido group and the C=C vibration of aromatic ring in the AMC moiety on A-ECNC surface respectively. It indicated the success coupling of fluorescent AMC onto the carboxylated surface of ECNC.

The EDTAD esterification of CNC certainly caused the changes of element compositions, and especially

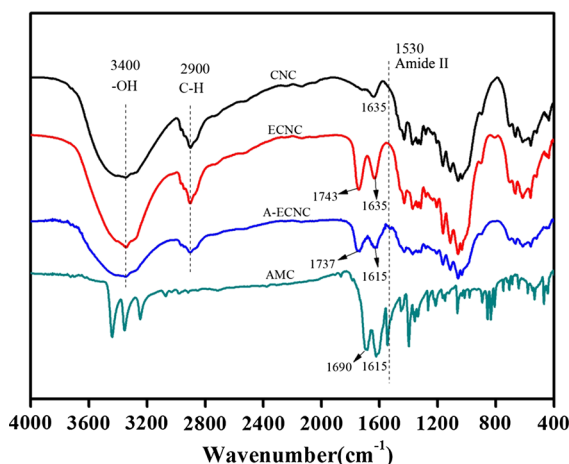


Fig. 2 FTIR spectra of carboxylated ECNC and fluorescent A-ECNC as well as AMC and CNC as comparison

the N element occurred. According to the elemental analysis results of ECNC, the degree of substitution (DS) for the surface hydroxyl groups can be calculated by the following Eq. (1) (Lin et al. 2016):

$$DS = \frac{N\% \div 2}{n_{OH}} \times 100\% \quad (1)$$

where $N\%$ is the determined content of N element in ECNC; n_{OH} is the hydroxyl content on the CNC surface, which is 1.5 mmol/g according to the previous report (Lin and Dufresne 2014). As shown in Table 1, the DS values of hydroxyl groups on CNC surface, which were calculated from elemental analysis results (Table S1), increased with an increase in the feeding molar ratio of EDTAD versus surface hydroxyl groups on CNC, indicating a controllability of EDTAD esterification. At the same time, the conductivity titration method has been applied to determine the carboxyl content of the ECNCs and their derivative A-ECNCs, and hence give the AMC content by the reduction of carboxyl content. Figures S1 and S2 depicted the conductimetric titration curves of ECNCs and A-ECNCs, respectively, and the surface carboxyl content (C_{COOH}) was calculated using the Eq. (2):

$$C_{COOH} = \frac{(V_2 - V_1)C}{\omega} \quad (2)$$

where V_1 and V_2 are the volumes of NaOH solution at the beginning and end positions of the turning point in the conductimetric titration curves; C is the concentration of NaOH aqueous solution as 0.03 mol/L in this work; and ω is the weight of the dried sample. Similar to the change tendency of DS values, the

results in Table 1 showed that the carboxyl contents (C_{COOH}) of ECNCs also increased with an increase in the feeding molar ratio of EDTAD versus surface hydroxyl groups on CNC, which could be controlled in the range from 0.66 mmol/g to 1.69 mmol/g. As usual, the surface carboxylation resulted in the increase of absolute value of negative ζ potential. CNC had a high ζ potential, which was corresponded to its sulfate groups and hydroxyl groups. However, as the S % was not changed correlated to the modification of CNC, it was considered that the sulfate groups on CNC were not take participate in the reactions that applied in this work. When the carboxyl content of ECNC was below 1.43 mmol/g, the ζ potential of the ECNCs kept at a level of about -38 mV. The effects of higher carboxyl content (i.e. 1.69 mmol/g for A-ECNC/40) on the spatial distribution and ionization equilibrium of carboxyl groups gave the ζ potential value of -41.2 mV. It indicated that there was enough colloid stability for the subsequent amidation with AMC. Hence, for the subsequent amidation of AMC with 5 times mole equivalent to the carboxyl content of ECNC, higher carboxyl content on the ECNC surface resulted in more conjugation of AMC. By determining the unreacted carboxyl contents of A-ECNCs and hence comparing with the corresponding ECNCs, the AMC contents (C_{AMC}) were obtained from the reduction of carboxyl contents. With an increase in the carboxyl content of ECNC, the AMC content of A-ECNC increased from 0.58 mmol/g to 1.07 mmol/g, namely a series of fCNC containing various loading-level of fluorescent moieties have been fabricated.

Table 1 The surface component, crystallinity index (I_c) and ζ potential of the CNC, ECNCs and A-ECNCs

| Sample | DS (%) | C_{COOH} (mmol/g) | I_c (%) | ζ potential (mV) | Sample | C_{AMC} (mmol/g) | I_c (%) |
|----------|----------|---------------------|-----------|------------------------|------------|--------------------|-----------|
| CNC | / | / | 87.6 | -33.7 ± 0.8 | / | / | / |
| ECNC/0.5 | 12.4 | 0.66 | 78.8 | -37.9 ± 0.5 | A-ECNC/0.5 | 0.58 | 78.3 |
| ECNC/2 | 24.2 | 0.92 | 78.3 | -37.5 ± 0.8 | A-ECNC/2 | 0.69 | 70.6 |
| ECNC/4 | 29.3 | 1.02 | 78.7 | -37.7 ± 0.9 | A-ECNC/4 | 0.76 | 72.3 |
| ECNC/10 | 32.4 | 1.12 | 75.4 | -37.3 ± 0.7 | A-ECNC/10 | 0.81 | 71.5 |
| ECNC/20 | 42.0 | 1.43 | 78.6 | -38.1 ± 0.6 | A-ECNC/20 | 0.94 | 67.9 |
| ECNC/40 | 50.5 | 1.69 | 74.0 | -41.2 ± 0.6 | A-ECNC/40 | 1.07 | 66.1 |

The DS , C_{COOH} and C_{AMC} represented the degree of substitution of surface hydroxyl groups on CNC, the carboxyl content of ECNC and the AMC content of A-ECNC, respectively

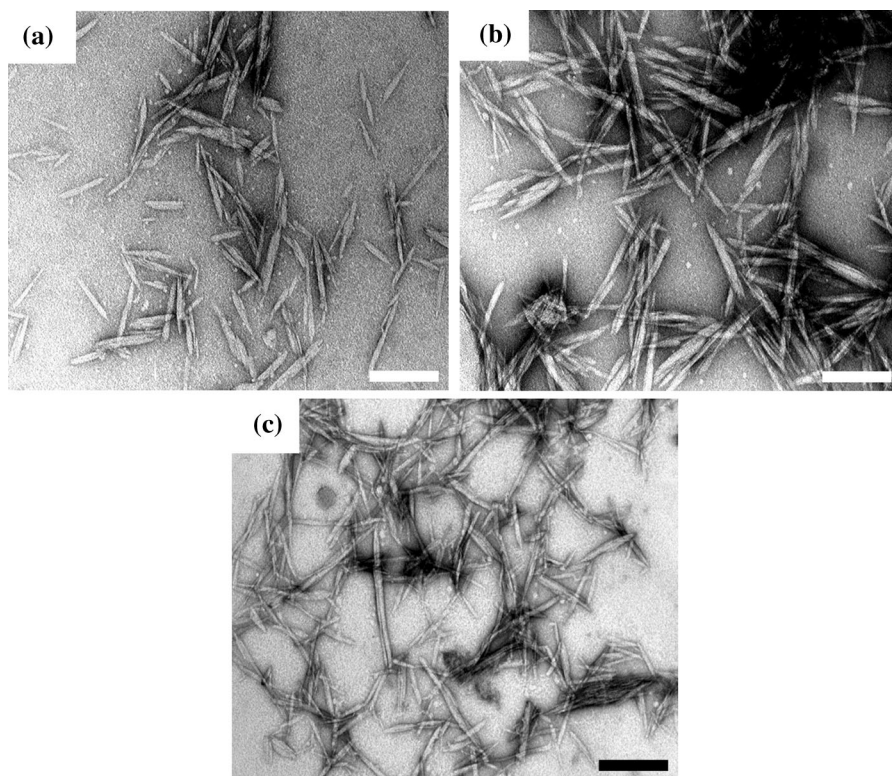


Fig. 3 TEM images of CNC (a), carboxylated ECNC (b) and fluorescent A-ECNC (c) (Scale bar 200 nm)

Structure of EDTAD-esterified and fluorescent cellulose nanocrystals

The chemical modification was required to keep the rod structure and high crystallinity of CNC as far as possible. Firstly, the effect of EDTAD esterification on the CNC crystallinity was investigated by the XRD patterns of Figure S3. As expected, the resultant ECNCs inherited the Cellulose I structure of the CNC, even at a high esterification degree of EDTAD, which was similar to our previous results on the anhydride esterification of CNC surfaces (Chen et al. 2009; Gan et al. 2017; Lin et al. 2009, 2012b). At the same time, the crystallinity index (I_c) values of the ECNC were close to that of CNC, indicating a preservation of high crystallinity and surface integration (Segal et al. 1959). Furthermore, as shown in Figure S4 and Table 1, all the fluorescent A-ECNCs also exhibited the Cellulose I character and the analogous I_c values. Herein, the obvious reduction of diffraction intensities as well as the slight decrease of I_c values might be ascribed to the fact that the composition changes and newly topological structure on the CNC surface after

EDTAD esterification and subsequent AMC amidation interfered the diffraction behaviors of cellulose crystals. On the other hand, the TEM images of CNC, ECNC and A-ECNC in Fig. 3 verified that the EDTAD esterification and subsequent AMC conjugation had no obvious influence on the rod morphology, and showed comparable diameter and length, i.e. the of CNC, ECNC and A-ECNC were respectively 135 ± 30 , 145 ± 40 and 147 ± 35 nm while corresponding diameters were respectively 14 ± 5 , 14.5 ± 4.5 and 15 ± 3.5 nm. As well-known, the TEMPO oxidization is a conventional method to prepare carboxylated CNC, but the carboxylation degree was usually limited in the range of $0.5 \sim 0.9$ mmol/g (Abou-Zeid et al. 2015; Araki et al. 2001; Buffa et al. 2016; Jin et al. 2016; Lin et al. 2012a; Yang et al. 2013). Although many attempts have been made to enhance carboxyl contents of TEMPO-oxidation and also reached 1.6 mmol/g that was equivalent to the highest value of EDTAD esterification in this work, severe oxidation together with the presence of alkali resulted in the decrease of size, the changes of morphology, and the damage and

transformation of crystalline (Montanari et al. 2005). As a result, the EDTAD esterification might be used to achieve highly carboxylated degree of CNC surface with as less damage of crystalline structure and surface integration as possible. Furthermore, the preservation of rod morphology and crystalline structure might provide a rigid foundation with a high aspect ratio to locate the moieties of ethylenediaminetetraacetic acid and the conjugated AMC molecules, and formed a topological distribution outward spreading from the CNC surface, which was expected to reduce the approaching possibility of fluorescent moieties and hence inhibit quenching.

Fluorescent property of fluorescent cellulose nanocrystals

Figure 4 depicts the effects of the AMC content on the fluorescence spectra of A-ECNC as well as the spectra of AMC, CNC and ECNC as comparison. Firstly, the AMC exhibited a predominant peak of fluorescence at 445 nm while the CNC and ECNC showed the weak peaks at 430 nm. Combined with the results about no absorption of CNC and ECNC in the UV–Vis spectra in Figure S5, the peaks at 430 nm of CNC and ECNC in Fig. 4 might be ascribed to the diffraction of

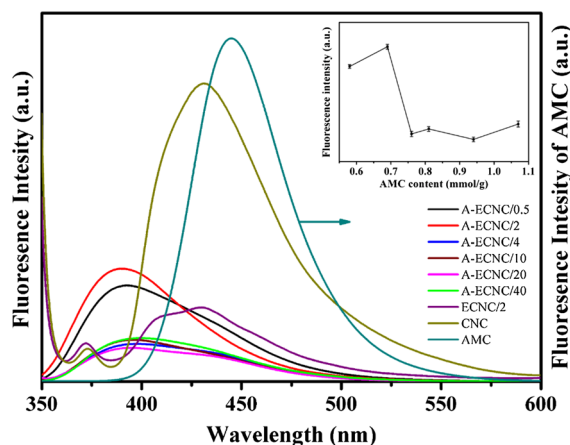


Fig. 4 Fluorescence spectra of AMC, CNC, ECNC/2 (carboxyl content 0.92 mmol/g) and A-ECNC with various AMC contents using the excitation wavelength of 350 nm for AMC and 325 nm for A-ECNCs, CNC and ECNC, and the change of fluorescence intensity at 390 nm of A-ECNC to the AMC content (inserted picture). (The peak of the AMC fluorescence at 430 nm was very predominant in contrast with those of the other specimens, and the peak intensity of AMC corresponded to the right vertical axis with greater scale)

excitation light by cellulose crystalline structure. Furthermore, the EDTAD esterification and subsequent AMC conjugation resulted in an obvious decrease of peak at 430 nm for ECNC and even the absence for A-ECNC, which also verified the diffraction nature of the peak at 430 nm because the topological structure on the modified CNC surface interfered this kind of diffraction behaviors. After conjugating AMC onto ECNC, the peak of the AMC fluorescence shifted from 445 nm to 390 nm due to the formation of amido bond and the interference of unreacted carboxyl groups in A-ECNC. However, when the free AMC was only physically mixed with acetic acid or ECNC, such blue shift could not be observed in Figure S6, indicating that the steric effects derived from the chemical conjugation between AMC and ECNC played a key role. At the same time, with an increase of AMC content in A-ECNC, the fluorescence intensity at 390 nm of the A-ECNCs firstly kept a higher level and the A-ECNC/2 with the AMC content of 0.69 mmol/g showed the maximum value. Thereafter, when the AMC content was higher than 0.76 mmol/g, the fluorescence intensity at 390 nm drastically reduced to 1/3 in contrast to that of A-ECNC/2. Since all amidated AMC molecules should crowded in the space near to the surface of nanoscaled CNC, the increase of AMC content inevitably shortened the distance among AMC molecules and hence caused self-quenching to reduce fluorescence intensity. Therefore, the A-ECNC/2 with the highest fluorescence intensity was selected for next research of ion detection.

Usually, the self-quenching of fluorescent molecules occurs with an increase of its concentration. As shown in Figure S7, with an increase of concentration, the fluorescent intensities of free AMC molecules firstly increased and reached the highest intensity at 0.03 mmol/L, and then dramatically declined until almost totally quenching at 0.5 mmol/L. However, Fig. 5 depicted the distinct dependence of the fluorescence intensity at 390 nm upon the A-ECNC/2 concentrations. Interestingly, with an increase of fluorescent A-ECNC/2 concentration in a range of 0.02% w/v to 0.5% w/v equivalent to the concentrations range of AMC as ca. 0.14 mmol/L ~ ca. 3.45 mmol/L, the fluorescence intensities at 390 nm maintained at an almost constant plateau after an initial enhancement at 0.06% w/v (the equivalent AMC concentration as ca. 0.41 mmol/L). The

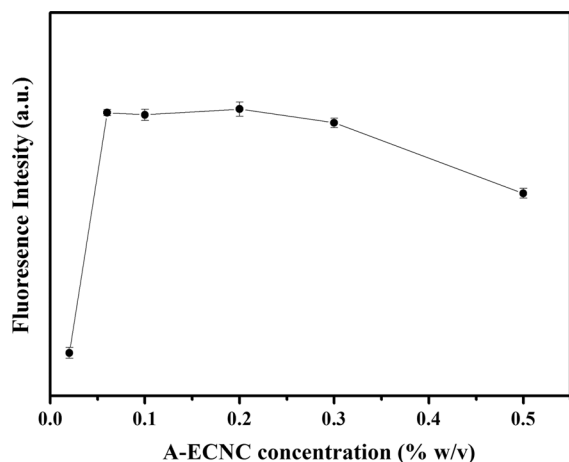


Fig. 5 Dependence of the fluorescence intensity at 390 nm upon the concentrations of A-ECNC/2

independence of fluorescence intensities upon the fluorescent A-ECNC concentration might contributed the additional advantages to optical detection. It might be ascribed to the fact that the topological structure outward spreading from the surface of rigid CNC provided steric separation for the surface anchored AMC moieties while the relative slow motion and colloid stability of nanoscaled particles reduced the approaching among A-ECNCs in suspension, which inhibited the quenching of fluorescent moieties. Furthermore, the steric separation effects of the topological structure outward spreading from the surface of rigid CNC was also verified by the quantum efficiency determination of A-ECNC/2 in the solid state. The quantum efficiency of solid A-ECNC/2 could reached 24.07%, and was comparable with that of the A-ECNC/2 suspension as 16.85%. Compared with the suspension, the higher quantum yield of A-ECNC/2 in dry state might be ascribed to the fact that the quenching effect of the solvent molecules towards fluorescent moieties was absent. (Bhavaya et al. 2018; Nagaraja et al. 2015; Sidarai et al. 2016).

Selective quenching of fluorescent cellulose nanocrystals towards metal ions

The concentration of 0.1% w/v was used to investigate the ion quenching behaviors of A-ECNC/2 with a AMC content of 0.69 mmol/g. The concentrations of all metal ions were set as 20 ppm, and the metal ions included Cu^{2+} , Co^{2+} , Ba^{2+} , Mg^{2+} , Ca^{2+} , Zn^{2+} , Mn^{2+} , Pb^{2+} , Hg^{2+} , Fe^{3+} , Na^+ and K^+ . Figure 6

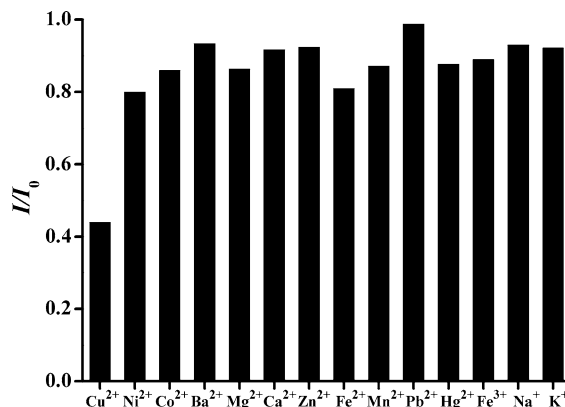


Fig. 6 Relatively fluorescence intensities at 390 nm (I/I_0) of A-ECNC/2 under the conditions of various metal ions, which derived from the fluorescence spectra in Figure S8 using the excitation wavelength of 325 nm for the mixing systems containing A-ECNC/2 and metal ions

depicted the relatively fluorescence intensities at 390 nm (I/I_0) of A-ECNC/2 under the conditions of various metal ions. Obviously, the introduction of metal ions led to the decrease of I/I_0 values in varying degrees, but the reduction extent caused by Cu^{2+} was very predominant. As well-known, the synergistic chelation of the carboxyl group and nitrogen atoms in molecule structure contributed a good selectivity to Cu^{2+} (He et al. 2018; Wu and Yan 2017). In this case, the predominant decrease of I/I_0 value for the system of Cu^{2+} and A-ECNC/2 was ascribed to the fact that the spatial distribution of carboxyl groups in ethylenediaminetetraacetic acid moieties and the amido bonds, which were formed in the conjugation of AMC and ECNC, could efficiently bind and enrich the Cu^{2+} from aqueous solution onto the A-ECNC surface.

Quantitative detection of Cu^{2+} using fluorescent cellulose nanocrystals

The predominant chelation of A-ECNC with Cu^{2+} showed a potential of Cu^{2+} detection in aqueous system. Figures 7a and 8a depicted the fluorescence spectra of A-ECNC/2 (0.1% w/v) in the aqueous systems containing 0 ~ 160 ppm Cu^{2+} . Obviously, there were two types of fluorescence spectra while the alternation happened at the Cu^{2+} concentration ($c_{\text{Cu(II)}}$) of 16 ppm, namely the unimodal spectra for the $c_{\text{Cu(II)}}$ below 16 ppm and the bimodal spectra after the $c_{\text{Cu(II)}}$ reached 16 ppm. Furthermore, Figs. 7b and 8b presented two linear correlations between

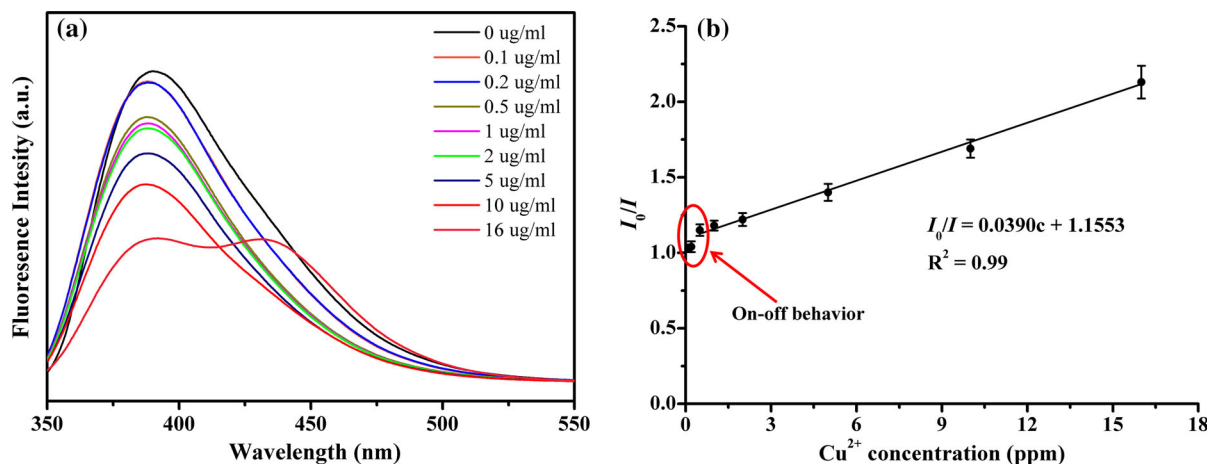


Fig. 7 Fluorescence spectra (a) of A-ECNC/2 in the aqueous systems containing 0–16 ppm Cu²⁺ using the excitation wavelength of 325 nm, and the derived Stern–Volmer plot (b) for the quantitative detection of the Cu²⁺ concentration below 16 ppm

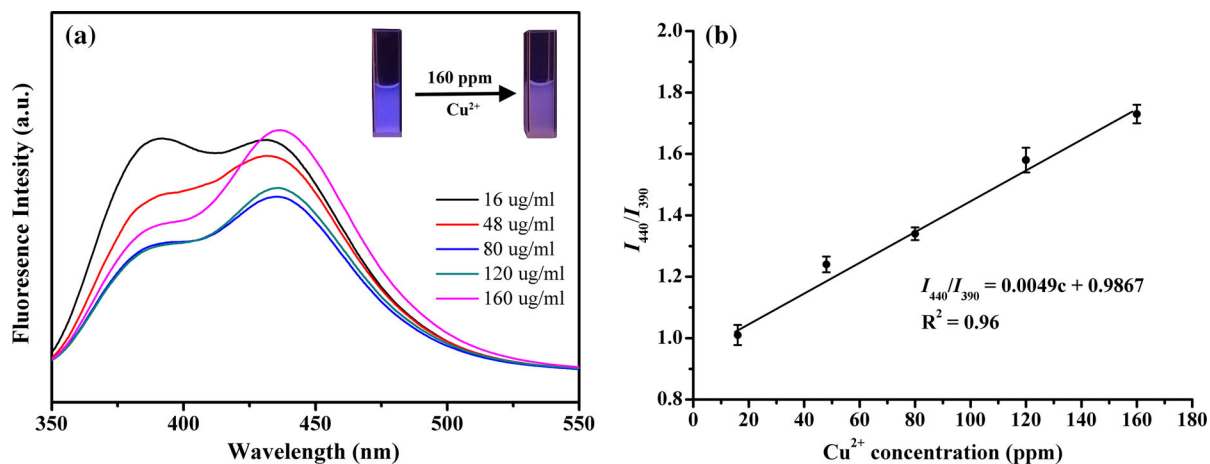


Fig. 8 Fluorescence spectra (a) of A-ECNC/2 in the aqueous systems containing 16–160 ppm Cu²⁺ using the excitation wavelength of 325 nm, and the derived dependence of the ratio

fluorescence signals and Cu²⁺ concentration, i.e. the fluorescence attenuation ratio at 390 nm (I_0/I) in 0.5–16 ppm of Cu²⁺ concentration and the ratio of fluorescence intensity at 440 nm versus 390 nm (I_{440}/I_{390}) in 16–160 ppm of Cu²⁺ concentration. In addition, it was worthy of noting that an on–off behavior of the A-ECNC/2 fluorescence happened at a critical Cu²⁺ concentration of 0.5 ppm, which was well consistent to the requirement of the Chinese Standard GB5749-2006 and the Guideline of Drinking-Water Quality (GDWQ) administrated by World Health Organization (WHO). On the other hand, under the ultraviolet radiation of 365 nm, high Cu²⁺ concentration, i.e. 160 ppm, would result in the color change of

of fluorescence intensity at 440 nm versus 390 nm (I_{440}/I_{390}) upon the Cu²⁺ concentration of 16–160 ppm (b)

A-ECNC from blue to purple, which could be observed by naked eyes. So the rapid and visualized evaluation method of drinking water quality might be developed.

Conclusions

In this study, a two-step reaction strategy was used to develop the fluorescent cellulose nanocrystals (fCNCs) for the selective and quantitative detection of Cu²⁺. The ethylenediaminetetraacetic dianhydride (EDTAD) was modified onto the CNC surface to achieve a controllable high carboxyl contents, which

further contributed to the regulation of conjugating density of fluorescent moieties and hence to the optimization of fluorescence intensity of fCNC. In this case, the mild EDTAD esterification and subsequent amidation with 7-amino-4-methylcoumarin (AMC) maintained rigid crystalline, rod morphology and surface integration, and hence led to a topological distribution of fluorescent moieties and other functional groups outward spreading from the CNC surface. It not only contributed to the independence of fluorescence intensity upon the fCNC concentrations in aqueous suspension, but also produced a higher quantum efficiency in the solid state. The selectivity of Cu^{2+} to quenching the resultant fCNCs was verified, and high Cu^{2+} concentration resulted in the visualized color change from blue to purple under ultraviolet radiation. Hence, two linear correlations between fluorescence signals and Cu^{2+} concentration were established for the quantitative detection of Cu^{2+} , i.e. the fluorescence attenuation ratio at 390 nm (I_0/I) in 0.5–16 ppm of Cu^{2+} concentration and the ratio of fluorescence intensity at 440 nm versus 390 nm (I_{440}/I_{390}) in 16–160 ppm of Cu^{2+} concentration. Interestingly, an on-off switch of the A-ECNC fluorescence intensity at 0.5 ppm of critical Cu^{2+} concentration showed a potential to the visualized evaluation of drinking water quality, and might meet the requirement of the Guideline of Drinking-Water Quality (GDWQ) administrated by World Health Organization (WHO) and Chinese standard GB5749-2006. Considering that the fluorescent moieties could facily alternated, this strategy was supposed to develop more kinds of fluorescent probes for extensive applications of optical imaging and detection.

Acknowledgments This work was financially supported by the National Natural Science Foundation of China (51373131), Fundamental Research Funds for the Central Universities (XDJK2016A017 and XDJK2016C033), Project of Basic Science and Advanced Technology Research, Chongqing Science and Technology Commission (cstc2016jcyjA0796), and Talent Project of Southwest University (SWU115034).

References

- Abou-Zeid RE, Hassan EA, Bettaieb F, Khiari R, Hassan ML (2015) Use of cellulose and oxidized cellulose nanocrystals from olive stones in chitosan bionanocomposites. *J Nanomater* 687490. <https://doi.org/10.1155/2015/687490>
- Araki J, Wada M, Kuga S (2001) Steric stabilization of a cellulose microcrystal suspension by poly(ethylene glycol) grafting. *Langmuir* 17:21–27. <https://doi.org/10.1021/la001070m>
- Awual MR (2017) New type mesoporous conjugate material for selective optical copper(II) ions monitoring & removal from polluted waters. *Chem Eng J* 307:85–94. <https://doi.org/10.1016/j.cej.2016.07.110>
- Bhavya P, Melavanki R, Kusanur R, Sharma K, Muttannavar VT, Naik LR (2018) Effect of viscosity and dielectric constant variation on fractional fluorescence quenching analysis of coumarin dye in binary solvent mixtures. *Luminescence* 33:933–940. <https://doi.org/10.1002/bio.3492>
- Buffa JM, Grela MA, Aranguren MI, Mucci V (2016) EPR spectroscopy applied to the study of the TEMPO mediated oxidation of nanocellulose. *Carbohydr Polym* 136:744–749. <https://doi.org/10.1016/j.carbpol.2015.09.094>
- Chen G, Dufresne A, Huang J, Chang PR (2009) A novel thermoformable bionanocomposite based on cellulose nanocrystal-graft-poly(epsilon-caprolactone). *Macromol Mater Eng* 294:59–67. <https://doi.org/10.1002/mame.200800261>
- Colombo L, Zoia L, Violatto MB, Previdi S, Talamini L, Sitia L, Nicotra F, Orlandi M, Salmona M, Recordati C, Bigini P, La Feria B (2015) Organ distribution and bone tropism of cellulose nanocrystals in living mice. *Biomacromolecules* 16:2862–2871. <https://doi.org/10.1021/acs.biomac.5b00805>
- Ding QJ, Zeng JS, Wang B, Gao WH, Chen KF, Yuan Z, Xu J (2017) Influence of binding mechanism on labeling efficiency and luminous properties of fluorescent cellulose nanocrystals. *Carbohydr Polym* 175:105–112. <https://doi.org/10.1016/j.carbpol.2017.07.068>
- Dong S, Roman M (2007) Fluorescently labeled cellulose nanocrystals for bioimaging applications. *J Am Chem Soc* 129:13810–13811. <https://doi.org/10.1021/ja076196l>
- Drew SC (2017) The case for abandoning therapeutic chelation of copper ions Alzheimer's disease. *Front Neurosci* 11:317. <https://doi.org/10.3389/fnins.2017.00317>
- Edwards JV, Fontenot KR, Haldane D, Prevost NT, Condon BD, Grimm C (2016) Human neutrophil elastase peptide sensors conjugated to cellulosic and nanocellulosic materials: part I, synthesis and characterization of fluorescent analogs. *Cellulose* 23:1283–1295. <https://doi.org/10.1007/s10570-016-0869-2>
- Fontenot KR, Edwards JV, Haidane D, Graves E, Citron MS, Prevost NT, French AD, Condon BD (2016) Human neutrophil elastase detection with fluorescent peptide sensors conjugated to cellulosic and nanocellulosic materials: part II, structure/function analysis. *Cellulose* 23:1297–1309. <https://doi.org/10.1007/s10570-016-0873-6>
- Gan L, Liao J, Lin N, Hu C, Wang H, Huang J (2017) Focus on gradientwise control of the surface acetylation of cellulose nanocrystals to optimize mechanical reinforcement for hydrophobic polyester-based nanocomposites. *ACS Omega* 2:4725–4736. <https://doi.org/10.1021/acsomega.7b00532>
- Grate JW, Mo K-F, Shin Y, Vasdekis A, Warmer MG, Kelly RT, Orr G, Hu DH, Dehoff KJ, Brockman FJ, Wilkins MJ

- (2015) Alexa fluor-labeled fluorescent cellulose nanocrystals for bioimaging solid cellulose in spatially structured microenvironments. *Bioconjugate Chem* 26:593–601. <https://doi.org/10.1021/acs.bioconjchem.5b00048>
- He GJ, Liu XL, Xu JH, Ji LG, Yang LL, Fan AY, Wang SJ, Wang QZ (2018) Synthesis and application of a highly selective copper ions fluorescent probe based on the coumarin group. *Spectrochim Acta Part A Mol Biomol Spectrosc* 190:116–120. <https://doi.org/10.1016/j.saa.2017.09.028>
- Huang JL, Li CJ, Gray DG (2013) Cellulose nanocrystals incorporating fluorescent methylcoumarin groups. *ACS Sustain Chem Eng* 1:1160–1164. <https://doi.org/10.1021/sc400074e>
- Jin E, Guo J, Yang F, Zhu Y, Song J, Jin Y, Rojas OJ (2016) On the polymorphic and morphological changes of cellulose nanocrystals (CNC-I) upon mercerization and conversion to CNC-II. *Carbohydr Polym* 143:327–335. <https://doi.org/10.1016/j.carbpol.2016.01.048>
- Kanumakala S, Boneh A, Zacharin M (2002) Pamidronate treatment improves bone mineral density in children with Menkes disease. *J Inherited Metab Dis* 25:391–398. <https://doi.org/10.1023/a:1020103901969>
- Lin N, Dufresne A (2014) Surface chemistry, morphological analysis and properties of cellulose nanocrystals with gradiented sulfation degrees. *Nanoscale* 6:5384–5393. <https://doi.org/10.1039/c3nr06761k>
- Lin N, Chen G, Huang J, Dufresne A, Chang PR (2009) Effects of polymer-grafted natural nanocrystals on the structure and mechanical properties of poly(lactic acid): a case of cellulose whisker-graft-polycaprolactone. *J Appl Polym Sci* 113:3417–3425. <https://doi.org/10.1002/app.30308>
- Lin N, Bruzzese C, Dufresne A (2012a) TEMPO-oxidized nanocellulose participating as crosslinking aid for alginate-based sponges. *ACS Appl Mater Interfaces* 4:4948–4959. <https://doi.org/10.1021/am301325r>
- Lin N, Huang J, Dufresne A (2012b) Preparation, properties and applications of polysaccharide nanocrystals in advanced functional nanomaterials: a review. *Nanoscale* 4:3274–3294. <https://doi.org/10.1039/c2nr30260h>
- Lin N, Geze A, Wouessidjewe D, Huang J, Dufresne A (2016) Biocompatible double-membrane hydrogels from cationic cellulose nanocrystals and anionic alginate as complexing drugs codelivery. *ACS Appl Mater Interfaces* 8:6880–6889. <https://doi.org/10.1021/acsami.6b00555>
- Ma X, Zhang Y, Huang J (2017) Surface chemical modification of cellulose nanocrystals and its application in biomaterials. *Pap Biomater* 2(4):34–57. <https://doi.org/10.12103/j.issn.2096-2355.2017.04.005>
- Mahmoud KA, Mena JA, Male KB, Hrapovic S, Kamen A, Luong JHT (2010) Effect of surface charge on the cellular uptake and cytotoxicity of fluorescent labeled cellulose nanocrystals. *ACS Appl Mater Interfaces* 2:2924–2932. <https://doi.org/10.1021/am100622z>
- Montanari S, Rountani M, Heux L, Vignon MR (2005) Topochemistry of carboxylated cellulose nanocrystals resulting from TEMPO-mediated oxidation. *Macromolecules* 38:1665–1671. <https://doi.org/10.1021/ma048396c>
- Nagaraja D, Melavanki RM, Patil NR, Geethanjali HS, Kusanur RA (2015) Solvent effect on the relative quantum yield and fluorescence quenching of a newly synthesized coumarin derivative. *Luminescence* 30:495–502. <https://doi.org/10.1002/bio.2766>
- Saleem M, Rafiq M, Hanif M, Shaheen MA, Seo S-Y (2017) A brief review on fluorescent copper sensor based on conjugated organic dyes. *J Fluoresc* 28:97–165. <https://doi.org/10.1007/s10895-017-2178-z>
- Seabra AB, Bernardes JS, Favaro WJ, Paula AJ, Duran N (2018) Cellulose nanocrystals as carriers in medicine and their toxicities: a review. *Carbohydr Polym* 181:514–527. <https://doi.org/10.1016/j.carbpol.2017.12.014>
- Segal L, Creely JJ Jr, Martin AE, Conrad CM (1959) An empirical method for estimating the degree of crystallinity of native cellulose using the X-ray diffractometer. *Text Res J* 29:786–794. <https://doi.org/10.1177/004051755902901003>
- Sidarai AH, Desai VR, Hunagund SM, Basanagouda M, Kadadevarmath JS (2016) Effect of solvent polarity on the fluorescence quenching of TMC molecule by aniline in benzene-acetonitrile mixtures. *Can J Phys* 94:1125–1132. <https://doi.org/10.1139/cjp-2016-0213>
- Sirbu E, Eyley S, Thielemans W (2016) Coumarin and carbazole fluorescently modified cellulose nanocrystals using a one-step esterification procedure. *Can J Chem Eng* 94:2186–2194. <https://doi.org/10.1002/cjce.22624>
- Sunasee R, Hemraz UD, Ckless K (2016) Cellulose nanocrystals: a versatile nanoplatform for emerging biomedical applications. *Expert Opin Drug Del* 13:1243–1256. <https://doi.org/10.1080/17425247.2016.1182491>
- Uriu-Adams JY, Keen CL (2005) Copper, oxidative stress, and human health. *Mol Aspects Med* 26:268–298. <https://doi.org/10.1016/j.mam.2005.07.015>
- Wu J-X, Yan B (2017) Visible detection of copper ions using a fluorescent probe based on red carbon dots and zirconium metal-organic frameworks. *Dalton Trans* 46:15080–15086. <https://doi.org/10.1039/c7dt03393a>
- Xue Y, Mou ZH, Xiao HN (2017) Nanocellulose as a sustainable biomass material: structure, properties, present status and future prospects in biomedical applications. *Nanoscale* 9:14758–14781. <https://doi.org/10.1039/c7nr04994c>
- Yang D, Peng XW, Zhong LX, Cao XF, Chen W, Sun RC (2013) Effects of pretreatments on crystalline properties and morphology of cellulose nanocrystals. *Cellulose* 20:2427–2437. <https://doi.org/10.1007/s10570-013-9997-0>
- Zhang L, Li Q, Zhou J, Zhang L (2012) Synthesis and photo-physical behavior of pyrene-bearing cellulose nanocrystals for Fe³⁺ sensing. *Macromol Chem Phys* 213:1612–1617. <https://doi.org/10.1002/macp.201200233>
- Zhao L, Li W, Plog A, Xu Y, Buntkowsky G, Gutmann T, Zhang K (2014) Multi-responsive cellulose nanocrystal-rhodamine conjugates: an advanced structure study by solid-state dynamic nuclear polarization (DNP) NMR. *Phys Chem Chem Phys* 16:26322–26329. <https://doi.org/10.1039/c4cp04096a>